Inverse Radiation Transport Problem Stability Analysis

David R. Anderson, John Mattingly

Dept of Nuclear Engineering, North Carolina State University, Burlington Engineering Labs, 2500 Stinson Drive, Raleigh, NC 2760, drander4@ncsu.edu, john_mattingly@ncsu.edu

INTRODUCTION

Inverse radiation transport may be used to characterize unknown radiation sources by estimating properties of the source term and transport medium based on radiation measurements. The inverse radiation transport problem comprises a number of variable parameters, such as source size, shape and geometric configuration, source composition and density, and shielding. The forward radiation transport engine consists of a deterministic transport solver that predicts the uncollided flux given the problem parameters. A nonlinear optimization routine modifies the transport model parameters to minimize the error between calculated detector response and measurements. Various combinations of radiation transport solvers, detectors, and optimization methods have been explored in previous work. [1]-[4] Solutions based solely on full-energy peaks in gamma spectroscopic measurements (i.e., on the uncollided gamma leakage) have exhibited multiple possible solutions. The stability of various solution methods has been explored, including an iterative calculation incrementing solution parameters and examining the solutions for minimum error compared to measurements, a least squares optimization, and a mesh adaptive search method (MADS).

PRELIMINARY CALCULATIONS

Ray Trace Verification

Aray-trace application based on the formulation described by Favorite [5] was developed. The ray-trace application for forward transport, developed in python, calculates the uncollided flux at a point detector from discrete gamma energies. The ray-trace is along a line of sight from the point detector back through the source. Multiple regions of source and attenuating medium can be modeled. The ray-trace application was verified using a model of a modified GODIVA sphere [1]. The modified GODIVA sphere is a 94.73% enriched uranium sphere of 8.704cm radius, with a surrounded by a 0.5cm thick lead sphere at 12.4cm with 0.2cm aluminum canning. Verification against the GODIVA model was a two-step process. The MCNP surface leakage was compared to the results of the analysis by Favorite [1] and was found to be within 5%. In step two, the ray-trace calculation was compared to MCNP calculations at a point detector 100cm from the center of the GODIVA sphere. The ray-trace results were within 5% of the MCNP results. The GODIVA model sources terms are given in Table I, while the results are shown in Tables II and III.

Table I. Modified GODIVA MCNP Model Sources.

Gamma Energy (keV)	Source Intensity (gammas/cm^{3}sec)
144.0	1.55E+05
186.0	8.11E+05
766.0	3.89E+01
1001.0	1.03E+02

Table II. GODIVA Results Ratios (RT = Ray-Trace)

Gamma Energy (keV)	Surface MCNP/Favorite	Leakage RT/MCNP	Detector Response at 100cm RT/MCNP
0.144	1.05	0.99	1.05
0.186	1.04	1.04	1.02
0.766	0.99	1.00	0.99
1.001	0.98	1.00	0.99

The ray-trace calculations were run using cross sections calculated by XCOM [6]. The calculations were run again with MCNP5 ENDF cross sections and were found to vary the results ratios by approximately 1%.

1D Representation Verification

Since the ray-trace application uses a 1D model, a calculation was performed to determine the accuracy of modeling a 3D geometry as an equivalent 1D geometry. The LLNL HEU sphere [7] was selected for this analysis. The sphere has a 3.151cm outer radius, and is composed of 94.5% enriched uranium. There is a 2.83cm deep conic frustrum void section. For the ray-trace calculation, the volume of this void was modeled as an equal volume spherical void of 1.60cm outer radius. The outer radius of the sphere was modeled at 3.151cm. The MCNP calculation was run using a 3D model that accurately represents the LLNL sphere. Figure 1 shows the MCNP 3D MCNP model and a representation of the 1Dray-trace model. Gamma sources are given below in Table III.

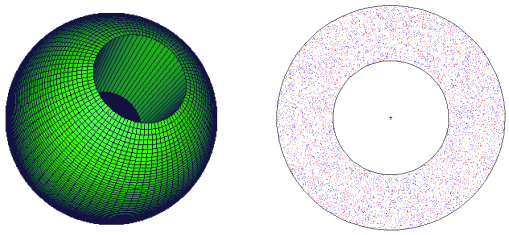

Fig. 1. LLNL HEU sphere, 3D (left), 1D (right)

Table III. LLNL HEU Sphere Sources.

Gamma Energy (keV)	Source Intensity (gammas/cm^{3}sec)
144.0	1.53E+05
186.0	8.00E+05
766.0	4.80E+01
1001.0	1.27E+02

The LLNL HEU sphere ray-trace results were compared to MCNP calculations. The uncollided flux at a detector 70.2 cm from the center of the sphere of the 1D concentric sphere model matched the 3D model results to within 3%, regardless of the placement of the point detector in relation to the conic void of the 3D MCNP model. This verified that the LLNL sphere could be acceptably modeled as a hollow sphere for a 1Dray-trace calculation. Table IV provides the results ratios of the ray-trace to MCNP calculations and show that the LLNL small HEU sphere can be accurately modeled as 1D concentric spheres of void region surrounded by source region.

Table IV. LLNL 1D vs 3D Results Ratios

Gamma energy (Mev)	Surface Leakage	Point Detector at 70.2cm
0.144	1.02	1.02
0.186	1.02	1.02
0.766	1.02	1.03
1.001	1.03	1.03

INVERSE TRANSPORT CALCULATIONS

The LLNL HEU sphere was used for calculations to determine the stability of solutions to the inverse transport calculation. The MCNP analysis results were used as the reference values and several techniques were explored in an attempt to determine the sphere parameters using an inverse analysis.

Inner and Outer Radius Iteration

An inverse transport calculation that iterated on problem parameters of source region inner and outer radius was first evaluated. Enrichment was set at its correct value of 93.5%. Gamma sources of Table II were used and inner and outer radius increments of 0.1 cm were evaluated in a nested loop calculation. The chi-squared error between the ray-trace results and the MCNP calculation was calculated at each step and collected in an array, where:

$$X^2 = \frac{1}{4}\sum_{i=1}^{4}(I_i^{mcnp} - I_i^{rayTrace})^2 / I_i^{mcnp} \qquad (1)$$

$where:$

$X^2 = Chi-squared\ error$

$i = gamma\ source\ line$

$I_i^{mcnp} = leakage\ flux\ from\ MCNP$

$I_i^{rayTrace} = leakage\ flux\ from\ RayTrace$

Figure 2 is a contour plot of the log of chi-squared plotted against inner and outer radius. The discrete minimums (in blue) are solutions, however, with a stepped iteration in 0.1 cm increments many valid solutions are passed over. Figure 2 shows that a very steep gradient exists close to the discovered solution values.

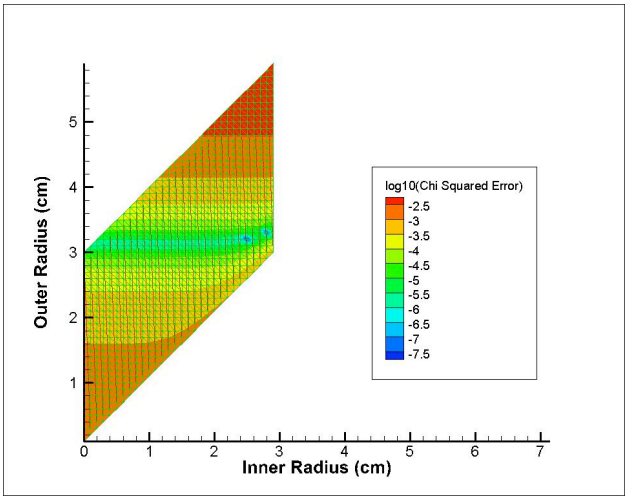

Fig. 2. 1001keV gamma solution plot, log(chi-squared) for values of outer and inner radius.

The plot of Figure 2 illustrates the problem solution using only the 1001keV uncollided flux. The uranium gamma lines are subject to significant self-shielding, therefore using uncollided flux for the analysis leads to a lack of information about the possible thickness of the HEU source region. Most uncollided gammas that reach the detector originate from near the surface of the sphere, especially for the lower energy ^{235}U gammas of 144keV

and 186keV. In actuality, a range of valid solutions exists, with a fixed outer radius and a continuum of values for the inner radius of the hollow sphere. The solution using only the 1001keV gamma line is least subject to self-shielding of the four gamma lines, however, a single solution for inner radius cannot be found.

Least Squares Optimization

To determine all of the valid solutions for the hollow sphere, an optimization routine was developed that used the SciPy least squares optimization routine scipy.optimize.leastsq [8]. This analysis determined the outer radii and inner radii that minimized the chi-squared error between the uncollided point detector flux from ray-trace and the reference MCNP calculation. Enrichment value was user specified in the python routine. Multiple values of enrichment can be specified in one analysis run. The python routine generated a solution for each enrichment value and created an output file for plotting the multiple solutions together. Gamma sources were specified using all four gamma lines, as given in Table III. A set of solutions that minimized the chi-squared error for each enrichment value specified was obtained. Solution parameters of outer radius and thickness were varied incrementally on both sides of the line of minimum chi-squared solution points. The resulting array of solution parameters and chi-squared were plotted. Figure 3 is a plot of log of chi-squared against outer radius and source region thickness for two different enrichments. The optimization routine shows significant difference in the error metric for small differences in enrichment levels, 95.0% and 93.5%. The calculated values of outer radius and enrichment are clearly defined. The only information about the thickness of the source region that could be determined is that it must be approximately 1cm thick or greater, as all thicknesses greater than 1cm are equally valid solutions due to self-shielding, as shown by the flat bottom of the 3D surfaces in Figure 3.

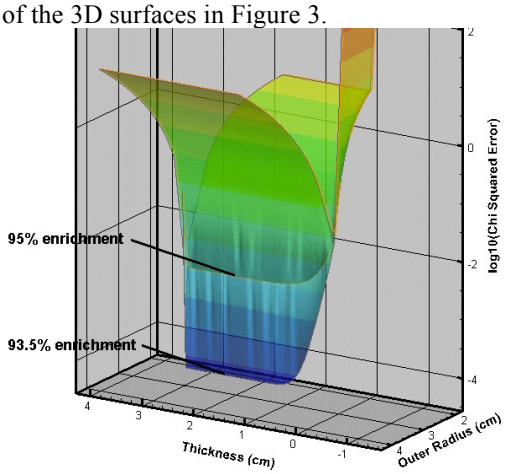

Fig. 3. Chi-Squared vs Outer Radius and Thickness using Least Square Optimization (95%, 93.5% enrichment)

Mesh Adaptive Direct Search

Finally, Mesh Adaptive Direct Search (MADS) was used to try to better characterize the solution. The open source code NOMAD [9] was used as the optimization tool. The NOMAD executable passes parameters to a "black box" executable, in this case a Python script that calculated the chi-squared error between the ray-trace analysis at the chosen parameters and the reference MCNP uncollided flux from each gamma line. Upper and lower bounds were specified for the outer radius, thickness, and enrichment as given in Table V,

Table V. NOMAD Upper and Lower Solution Bounds.

	Outer Radius	**Thickness**	**Enrichment**
Lower Bound	1.0	0.0	0.50
Upper Bound	6.0	4.0	0.97

An initial guess passed from NOMAD to the python routine for outer radius, thickness and enrichment. NOMAD was run with different initial guesses and with two different sets of constraint values to determine the sensitivity of the solution to different starting values. The results showed that while NOMAD consistently determined the outer radius and the enrichment of the LLNL sphere, it was inconsistent in the determination of the source region thickness. There is no noticeable correlation between the starting guess and the source region thickness determined by NOMAD. For each different set of starting data the MADS solver in NOMAD took a different path to the calculated minimum value of chi-squared error. Once it determined a minimum value and could not improve on that minimum within the calculation stopping criteria, the problem was solved. Again, a continuum of valid thicknesses is possible, but NOMADS was unable to improve on the previous solution methods. Table VI provides results of the determination of source thickness based on the starting guess that was input. Enrichment was determined to be 93.5% in each case and outer radius was determined to be 3.061cm (actual value 3.151cm). The last table entry was run with the initial guess equal to the correct values and did not calculate the correct inner radius of 1.60cm.

Table VI. MADS Determined Source Region Thickness

Initial Guess			NOMAD Solution
Outer Radius	**Thickness**	**Enrichment**	**Thickness**
1.00	0.00	0.50	2.896
2.00	0.00	0.50	2.106
3.00	0.00	0.50	3.051
3.00	1.00	0.50	1.499
4.00	2.00	0.50	2.695
5.00	3.00	0.50	3.036
3.15	1.55	0.935	2.330

Figure 4 graphically shows the MADS solution, with the blue markers representing solutions with the lowest chi-squared error. Starting guess values for the run shown in Figure 2 were:

outer radius = 3.0cm,
thickness = 0.0cm,
enrichment = 0.50 (50.0%)

The blue minimum error markers trace a continuous line of source region thickness solutions corresponding to an outer radius of 3.06 cm and 93.5% enrichment.

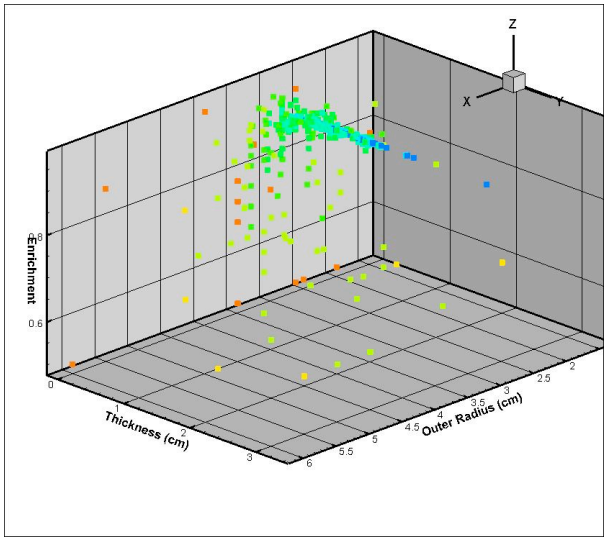

Fig. 4 NOMAD based MADS solution of outer radius, thickness and enrichment, with solution points color coded by chi-squared.

CONCLUSIONS

While the parameters of HEU sources with solid geometry can be reliably determined for values of outer radius and enrichment using uncollided flux measurements, the addition of more complicated geometry such as a hollow central region leads to solutions where outer radius and enrichment can be reliably determined, but little information can be determined about source region thickness. This is due primarily to the effect of self-shielding of the uranium gamma lines. Few uncollided gammas arrive at the detector from deep inside the source region. The addition of Compton continuum could provide data necessary to better determine the estimate of scattering material and therefore improve the estimate of source region thickness. However, thickness estimates may still be limited to bounding the source region thickness. Future work will involve the addition of a detector response function and collection of full spectrum leakage data to the ray-trace calculations.

ACKNOWLEDGEMENTS

This work was supported in part by the National Nuclear Security Administration Office of Nonproliferation and Verification Research and Development.

REFERENCES

1. J. FAVORITE, "Using the Schwinger Variational Functional for the Solution of Inverse Transport Problems," *Nuclear Science and Engineering*, **146**, 51-70 (2004).
2. K. BLEDSOE, J. FAVORITE, T. ALDEMIR, "Using the Levenberg-Marquardt Method for Solutions of Inverse Transport Problems in One- and Two- Dimensional Geometries", *Nuclear Technology*, **176**, 106-126 (2011)
3. J. MATTINGLY, D. J. MITCHELL, and L. T. HARDING, "Experimental Validation of a Coupled Neutron-Photon Inverse Radiation Transport Solver," *Nuclear Instruments and Methods in Physics Research A* **652**(1), 537-539, (2011)
4. J. MATTINGLY and D. J. MITCHELL, "A Framework for the Solution of Inverse Radiation Transport Problems," *Transactions on Nuclear Science* **57**(6), 3734-3743 (2010)
5. J. FAVORITE, K. BLEDSOE, D. KETCHESON, "Surface and Volume Integrals of Uncollided Adjoint Fluxes and Forward-Adjoint Flux Products" *Nuclear Science and Engineering,* **163,** 73-84 (2009)
6. M.J. Berger, J.H. Hubbell, S.M. Seltzer, J. Chang, J.S. Coursey, R. Sukumar, D.S. Zucker, and K. Olsen, XCOM: Photon Cross Sections Database, NIST Standard Reference Database 8, http://www.nist.gov/pml/data/xcom
7. W. WEBSTER, C. WONG, "Measurements of the Neutron Emission Spectra from Spheres of N, O, W, EXP, U-235, Exp U-238 and Exp Pu-239 Pulsed by 14Mev Neutrons," California University, Livermore, LL Laboratories (1976).
8. Numpy and Scipy Documentation, SciPy v0.12 Reference Guide (DRAFT), http://docs.scipy.org/doc
9. S. Le DIGABEL, C. TRIBES, C. AUDET, NOMAD User Guide Version 3.6.1, Technical Report G-2009-37, Les cahiers du GERAD, 2009.